Physics Letters A 384 (2020) 126535

Contents lists available at ScienceDirect

Physics Letters A

www.elsevier.com/locate/pla

Mass-imbalanced Bose-Einstein condensed mixtures in rotating perturbed trap

R. Kishor Kumar [a,b], A. Gammal [c], Lauro Tomio [b,*]

[a] Department of Physics, Centre for Quantum Science, and Dodd-Walls Centre for Photonic and Quantum Technologies, University of Otago, Dunedin 9054, New Zealand
[b] Instituto de Física Teórica, Universidade Estadual Paulista (UNESP), 01140-070, São Paulo, Brazil
[c] Instituto de Física, Universidade de São Paulo, 05508-090, São Paulo, Brazil

ARTICLE INFO

Article history:
Received 19 March 2020
Received in revised form 24 April 2020
Accepted 30 April 2020
Available online 8 May 2020
Communicated by B. Malomed

Keywords:
Binary mixture
Bose-Einstein condensate
Gross-Pitaevskii
Vortex patterns
Rubidium-cesium

ABSTRACT

We consider the mass-imbalanced sensibility for the emergence of vortex patterns in the Bose-Einstein condensed binary mixture of rubidium-cesium (^{85}Rb-^{133}Cs), confined in quasi-two-dimensional harmonic traps, with one species linearly perturbed in one direction. Non-dipolar coupled species are chosen to highlight mass symmetry effects. We first analyze the condensed mixture in the unperturbed non-rotating regime, where radial phase separation is verified in the immiscible regime, which occurs for large ratio between inter- and intra-species repulsive interactions. By going to the linear perturbed regime, the radial phase separation that occurs in the immiscible condition splits up with the two densities having their maxima at distinct positions. In the rotating regime of both unperturbed and perturbed cases, the minimum rotation is determined in terms of the inter-species interaction to observe vortex structures. In the immiscible regime a dramatic spatial interchange between the species is verified by increasing the rotation.

1. Introduction

The first reported experimental realization of a Bose-Einstein condensate (BEC) mixture with two hyperfine spin states of ^{87}Rb [1], and the corresponding experimental observation of vortices in this two-component hyperfine mixture [2], have motivated several other theoretical and experimental studies with BEC binary mixtures. Actually, following these works, it is been quite well established the observation and several studies with binary BEC mixtures having different hyperfine states, different atomic isotopes, as well as different atom-atom or atom-molecular mixtures [3–16]. Further, coreless vortices are also observed in the three-component order parameter with $F = 1$, for sodium condensates [17]. More related studies on vortices and vortex lattices observations, with particular focus on atomic systems having magnetic dipole moments, in which properties of quantum ferrofluids emerge, can also be found in the recent review by Martin et al. [18], where they discuss analytic treatments based on the Thomas-Fermi and variational approaches, as well as full numerical simulations. As verified, even with single atomic species, the studies on generating vortices in dipolar condensates lead to the appearance of a rich variety of vortex lattice structures [19]. In view of the actual experimental progress with ultracold dipolar atomic systems [14], one of the interesting aspects been considered on the properties of rotating dipolar mixtures, is the possibility for tuning the corresponding inter-species dipolar interactions [20]. The studies on vortex patterns in multicomponent BECs are also interesting due to different miscibility properties. Peculiar vortex structures can be verified in addition to the fundamental Abrikosov's triangular lattice [21], such as squared, striped, with domain walls, and rotating droplets [22–26]. When considering ring-trap geometry, the miscibility and stability requirements for binary atomic BECs with repulsive interactions was recently studied in Ref. [27]. More recently, within the investigations with binary mixtures of Bose-Einstein condensates, we noticed studies with massive core vortices [28], as well as the dynamics of vortex-bright-soliton spontaneous generation with small mass imbalance between the species [29].

The experiment with the ^{85}Rb-^{133}Cs mixture, reported of having three distinct density distributions, depending on the relative atom numbers in each component of BECs [8], was further analyzed by using the mean-field theoretical model [30]. From this analysis, it was observed that weak perturbations are provided by the tilt in the magnetic dipole trap, due to larger inelastic three-body losses, which affect the equilibrium density distributions, displaying different miscibility or phase separations. The tilt in the

* Corresponding author.
E-mail address: lauro.tomio@unesp.br (L. Tomio).

https://doi.org/10.1016/j.physleta.2020.126535
0375-9601/

magnetic dipole trap, having small differences between the species, was applied in one of the transverse direction, implying in a corresponding shift in the relative trap centers. Therefore, by applying a linear-trap perturbation, in addition to the harmonic trap in a cigar shaped trap, one can analyze the effect of the tilt in the magnetic dipole trap and corresponding density distributions. Further, one could also consider a linear-trap perturbation in two-dimensional coupled systems, to investigate the effect on the vortex structure patterns.

Motivated by a previous investigation with dipolar mixtures [20], in which a remarkable mass-imbalance sensibility was verified in the miscibility and vortex-pattern distribution of symmetric- and asymmetric-dipolar mixtures, the focus of the present paper is to study the mass-imbalance effect in the density phase separation and corresponding vortex pattern structure, by considering two non-dipolar species in which the mass symmetry effect can be more clearly evidenced by varying the associated two-body interactions. For that, in our study we select the non-dipolar coupled mixture ^{85}Rb-^{133}Cs due to the actual interest and experimental possibilities. With non-dipolar binary system, the mass-imbalance sensibility can be highlighted with simple non-perturbed and perturbed pancake-like traps. We should observe that, among the non-dipolar binary mixtures being studied in cold-atom laboratories, one can consider atomic elements with small mass difference, as two isotopes of rubidium [1] or two isotopes of cesium [31] or with large mass difference, as the binary mixture ^{85}Rb-^{133}Cs [8,9]. The first case, use to be investigated by model approximations where both species have identical masses [32]. However, in view of the observed mass-imbalance sensibility [20], we found appropriate to work with the second case where the mass difference cannot be neglected, such that relevant related properties on the miscibility and vortex structures can be pointed out. As verified, the more mass-symmetric BEC mixtures, as ^{87}Rb-^{85}Rb or the dipolar one ^{164}Dy-^{162}Dy, can show triangular, squared, striped, domain wall, and rotating droplets vortex-lattice structures regarding to the ratio between inter- and intra-species contact interaction. On the other hand, highly mass-imbalanced mixtures, such as ^{85}Rb-^{133}Cs, are more likely to present radial vortex-lattice patterns in the quasi-2D pancake-like configuration.

Our analysis is performed for a pancake-shaped trap configuration, with the trap frequencies $\omega_x = \omega_y \equiv \omega_\rho \ll \omega_z$ (aspect ratio $\lambda \equiv \omega_z/\omega_\rho \gg 1$), in which the underlying three-dimensional (3D) system can be reduced to a two-dimensional (2D) one. The effect of a perturbation in the original pancake-like harmonic trap is verified by adding a linear shift of one of the species along the x-direction. In our study, we assume fixed and repulsive the intra-species interactions, $a_{11} = a_{22}$, varying the inter-species one, a_{12}, from attractive to repulsive interactions, which will correspond in going from miscible to immiscible regimes of the mixture. The critical rotation frequencies to generate vortices in the coupled system are verified by introducing rotation in the trapped system. We have also verified the density distribution of the two species and how the dynamics of vortices is being modified by increasing the rotation. Guided by a previous analysis [20], we understand that highly mass-imbalanced mixtures in non-perturbed harmonic trap and without rotation should present radially phase-separated distributions in the immiscible regime where the inter-species a_{12} is positive and larger than the repulsive intra-species ones, a_{ii} ($i = 1$ and 2). After verifying the effect of the shift-perturbation in one of the trapped species (non-rotating case), we study the non-perturbed and perturbed rotating mixtures, in order to observe how the radial separations and vortex-pattern structure are affected by the mass asymmetry, with particular focus in the immiscible regime.

In the next Sect. 2, we have the mean-field approach applied to rotating binary mixtures in a pancake-like trap, which includes a discussion on miscibility properties. In Sect. 3, after a brief discussion on our numerical procedure, we present our main results. Finally, in Sect. 4 we have a summary with concluding remarks.

2. Mean-field model for rotating binary BEC

In our approach for the coupled BEC system, the two atomic species $i = 1, 2$ with masses m_i are assumed with the same number of atoms $N_i \equiv N$, confined in strongly pancake-shaped harmonic traps with fixed aspect ratios $\lambda \equiv \lambda_i = \omega_{i,z}/\omega_{i,\perp} = 10$, where $\omega_{i,z}$ and $\omega_{i,\perp}$ are, respectively, the longitudinal and transverse trap frequencies for the species i. We further assume the intra-species scattering lengths are identical and fixed for both species, with $a_{11} = a_{22} = 150a_0$ (a_0 is the Bohr radius), such that the relative strength is controlled by the inter-species interaction a_{12}. The coupled Gross-Pitaevskii (GP) equation is cast in a dimensionless format, with energy and length units given, respectively, by $\hbar\omega_{1,\perp}$ and $l_{\perp,1} \equiv \sqrt{\hbar/(m_1\omega_{1,\perp})}$. By taking the first species as the reference in our unit system, in the next we have $\omega_\perp \equiv \omega_{1,\perp}$ and $l_\perp \equiv l_{\perp,1}$. Correspondingly, the space and time variables are such that $\mathbf{r} \to l_\perp \mathbf{r}$ and $t \to \tau/\omega_\perp$, when going from full-dimension to dimensionless quantities. Within these units, for simplicity we first adjust both trap frequencies as $m_2\omega_{2,\perp}^2 = m_1\omega_{1,\perp}^2$, such that the dimensionless non-perturbed 3D trap for both species have the same expression given by

$$V_{i,3D}(\mathbf{r}) = \frac{1}{2}(x^2 + y^2 + \lambda^2 z^2) \equiv V_0(x, y) + \frac{1}{2}\lambda^2 z^2, \tag{1}$$

where $V_0(x, y)$ is the 2D non-perturbed harmonic oscillator. By adjusting the trap frequencies as above, we have no explicit mass-dependent factor in the trap potential. Next, we also assume a large value for the aspect ratios λ, which allows us to reduce the original 3D formalism to a 2D one, by the usual factorization for the 3D wave function, $\psi_i(x, y, \tau)\chi_i(z)$, where $\chi_i(z) \equiv (\lambda_i/\pi)^{1/4} e^{-\lambda_i z^2/2}$. In this case, the ground-state energy for the harmonic trap in the $z-$direction is a constant factor to be added in the total energy. It is safe to assume a common mass-independent transversal wave-function for both components, with $\lambda_i = \lambda$, as any possible mass dependence can be absorbed by changing the corresponding aspect ratio. This approach for the reduction to 2D implies that we also need to alter the nonlinear parameters accordingly, as the integration on the $z-$direction will bring us a $\lambda-$dependence in the non-linear parameters. So, the corresponding coupled 2D GP equation in the rotating frame is given by

$$\mathrm{i}\frac{\partial\psi_i}{\partial\tau} = \left\{\frac{-m_1}{2m_i}\left(\frac{\partial^2}{\partial x^2} + \frac{\partial^2}{\partial y^2}\right) + V_i(x, y) - \Omega L_z + \sum_{j=1,2} g_{ij}|\psi_j|^2\right\}\psi_i, \tag{2}$$

where $\psi_i \equiv \psi_i(x, y, \tau)$ and $\psi_i' \equiv \psi_i(x', y', \tau)$ are the components of the total 2D wave function, normalized to one, $\int_{-\infty}^{\infty} dx dy\, |\psi_i|^2 = 1$. L_z is the angular momentum operator with Ω the corresponding rotation parameter (in units of $\omega_\perp$), which is common for the two components. The two-body contact interactions, which are related to the scattering lengths a_{ij} for the species $i, j = 1, 2$ (where $a_{ij} = a_{ji}$) are given by

$$g_{ij} \equiv \sqrt{2\pi}\lambda\frac{m_1 a_{ij} N_j}{\mu_{ij} l_\perp}, \tag{3}$$

where $\mu_{ij} \equiv m_i m_j/(m_i + m_j)$ is the reduced mass; and we assume $a_{11} = a_{22}$, with the same number of atoms for both species, $N_1 = N_2$. In the next, the length unit will be adjusted to $l_\perp = 1\ \mu\mathrm{m} \approx 1.89 \times 10^4 a_0$, where a_0 is the Bohr radius, such that a_{ij}

can be conveniently given in terms of a_0. $V_{i=1,2}(x, y)$ is the external potential provided by the harmonic trap, which we assume that the component $i = 1$ can be perturbed by the addition of a linear trap along x. It can be expressed by

$$V_i(x, y) = \frac{x^2 + y^2}{2} + \nu_i x = \frac{(x + \nu_i)^2 + y^2}{2} - \frac{\nu_i^2}{2}, \tag{4}$$

where $\nu_{i=1,2} = 0$ for the non-perturbed case; and $\nu_1 = 1$, with $\nu_2 = 0$ for the perturbed case. As indicated by the above Eq. (4), in the perturbed case the center of the harmonic trap for the species $i = 1$ is shifted to $x = -1$.

A relevant property to be considered for coupled mixtures is the miscibility of the components. By following a simplified energetic approach derived in Ref. [33] for homogeneous systems, one can characterize the transition between miscible and immiscible states for systems with repulsive two-body interactions by a criterion, which is independent on the condensate atom numbers or trap sizes. Considering this criterion, a coupled system enters in an immiscible regime for $G_{12}^2 > G_{11}G_{22}$, where G_{ij} are given by the ratio between the corresponding two-body scattering lengths a_{ij} and reduced masses μ_{ij}, given by $G_{ij} \equiv 2\pi\hbar^2 a_{ij}/\mu_{ij}$. This condition to enter in an immiscible regime, which also corresponds to $g_{12}^2 > g_{11}g_{22}$ [using Eq. (3)], for $a_{11} = a_{22} > 0$, can define a threshold parameter δ, given by

$$\delta \equiv \frac{a_{12}}{a_{11}} > \frac{2\sqrt{m_1 m_2}}{m_1 + m_2}, \tag{5}$$

where the right-hand-side is the mass-dependent critical value for the miscible-immiscible transition of homogeneous mixture. In the present case, this critical value is $\delta \simeq 0.975$, which is not far from the equal-mass case, such that we can still consider $\delta = 1$ as the approximate value for the transition.

When considering general non-homogeneous coupled mixture, the miscibility was further studied in Ref. [34], where a convenient parameter was defined for the miscibility, using the overlap between the densities, which for the present 2D case is given by

$$\eta = \int |\psi_1||\psi_2|\, dxdy = \int \sqrt{|\psi_1|^2|\psi_2|^2}\, dxdy, \tag{6}$$

where both ψ_1 and ψ_2 are normalized to one. It implies in $\eta = 1$ for the complete overlap between the two densities and zero in the opposite limit. Equivalent to the above definition, one can also find some other suggestions, as in Refs. [35,36], used as criterion to separate the miscible and immiscible phases, based on the overlap of the densities.

3. Results for non-rotating and rotating binary mixtures in non-perturbed and perturbed traps

We start by a brief explanation on our numerical approach to obtain the results for general mass-imbalanced binary mixtures. As one can verify from the formalism given in section 2, the mass symmetry appears explicitly in the kinetic-energy terms (reflected in the second component of the coupled system), with the mass-imbalance factor given by $(m_2/m_1 - 1)$. By assuming the species $i = 2$ as the larger-mass component of the mixture, in case of ^{85}Rb-^{133}Cs the mass-imbalanced factor is 0.5647. For the atom-atom interactions, we assume enough large repulsive intra-species scattering lengths $a_{11} = a_{22} = 150a_0$, remaining the inter-species one to be explored from attractive to larger repulsive values, through the parameter δ, given by (5). The 2D coupled mean-field equation, was solved by the split time-step Crank-Nicolson method with an appropriate algorithm discretization as

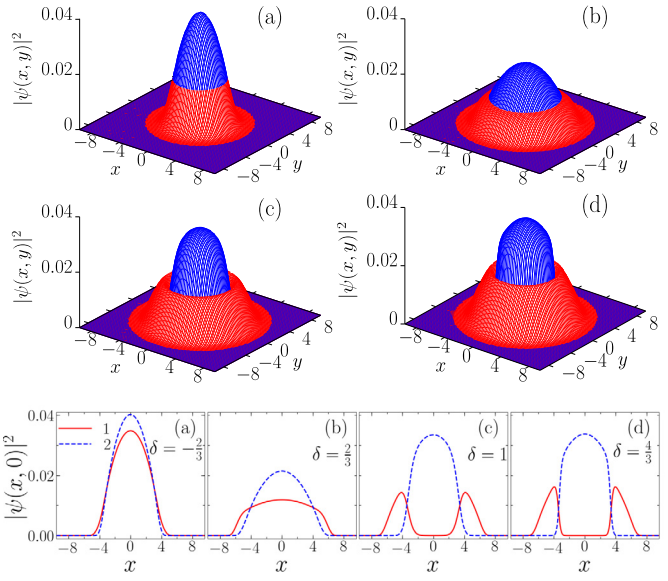

Fig. 1. The non-perturbed non-rotating ($\Omega = 0$) harmonically confined, with aspect ratio $\lambda = 10$, 2D component densities (units of $l_\perp^{-2}$) are shown for the mixture ^{85}Rb-^{133}Cs, using surface plots in the upper (a)-(d) panels, in which $a_{12} = -100a_0$ (a), $a_{12} = 100a_0$ (b), $a_{12} = 150a_0$ (c), and $a_{12} = 200a_0$ (d). With $a_{11} = a_{22} = 150a_0$ fixed, the corresponding δ are indicated inside the lower panels, in which the respective central densities ($y = 0$) are presented along the $x-$direction (units of $l_\perp$), with the red-solid line referring to ^{85}Rb (element 1) and the blue-dashed line to ^{133}Cs (element 2). (For interpretation of the colors in the figures, the reader is referred to the web version of this article.)

described in Ref. [37]. As our aim was to study some ground state properties of the mass-imbalanced coupled system, we have mainly concerned with time-independent solutions. As to confirm the stability of our results in the calculation of non-rotating ground states, for the initial component wave functions used in the time-dependent equation (2), we assume a simplified Gaussian expression, given by $\psi_{i,0}(x, y) = (1/\sqrt{\pi})\exp\left[-(x^2 + y^2)/2\right]$. However, when studying rotational properties, for the initial component wave-functions we consider these component wave functions with a single vortex at the center, modulated by a random phase at different space points, as

$$\psi_{i,0}(x, y) = \frac{(x + \mathrm{i}y)}{\sqrt{\pi}} \exp\left(-\frac{x^2 + y^2}{2} + 2\pi\,\mathrm{i}\mathcal{R}(x, y)\right), \tag{7}$$

where $\mathcal{R}(x, y)$ is a random number in the interval $[0, 1]$. This procedure, found to be simpler than the one used in [26], has been shown to be relevant to address convergence issues, and to overcome the impact of the initial condition on the final vortex solutions [37]. Within our dimensionless variables, for the coupled system we use space step size 0.05 and time step 0.0005, with the stability being confirmed by performing time evolution from $t = 0$ up to $t = 2000$ (units $\omega_\perp^{-1}$).

In the next sub-sections, our main numerical results are detailed, in which the unperturbed case, which can be found in several other studies, as already mentioned, is reported to serve as reference to the other results we are presenting for the perturbed case, as well as for the rotating cases.

3.1. Non-rotating, non-perturbed and perturbed system

First, we present in Fig. 1 the results for the density distributions of the two components within non-perturbed harmonic traps, in order to verify the corresponding miscibility properties in non-rotating conditions, $\Omega = 0$. In the upper (a)-(d) four panels, by using 2D surface plots, we show how the corresponding

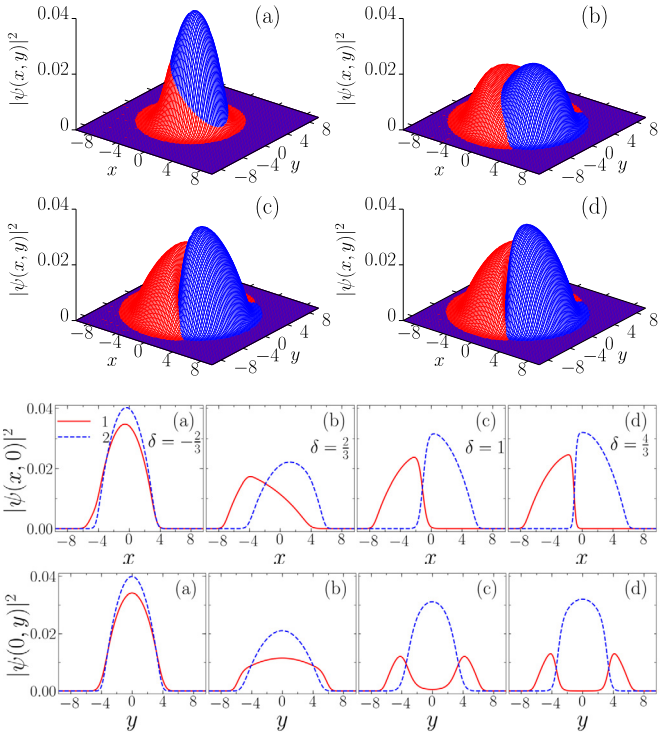

Fig. 2. With the harmonic trap linearly perturbed in the $x-$direction ($\nu_1 = 1, \nu_2 = 0$), this figure shows the corresponding panels presented in Fig. 1. Except for the perturbation, all the other parameters are the same as used in Fig. 1. In this case, the two lower rows of panels are for $|\psi_i(x,0)|^2$ and $|\psi_i(0,y)|^2$, along the x and y directions, respectively.

densities of the two elements [^{85}Rb and ^{133}Cs] are spatially distributed, for different inter-species scattering lengths, and confined in harmonic traps with the same aspect ratio $\lambda = 10$. In the lower (a)-(d) four panels we show the respective densities [corresponding to the (a)-(d) upper panels] along the $x-$direction, for $y = 0$. In all the results, the intra-species scattering lengths are kept fixed, $a_{11} = a_{22} = 150a_0$, with the inter-species fixed at different values at each panel, such that in the panels (a) we have $a_{12} = -100\,a_0$; in panels (b), $a_{12} = 100\,a_0$; in panels (c), $a_{12} = 150\,a_0$; and, in panels (c), $a_{12} = 200\,a_0$. The plots are showing the miscibility to immiscibility transition for non-rotating ($\Omega = 0$) binary BEC mixture confined in harmonic trap with aspect ratio $\lambda = 10$. The resulting distribution is such that, as δ becomes larger than 1, the massive component ($i = 2$, the ^{133}Cs) remains with the maximum in the center, with the density of the lighter one being reduced to a minimum in the center. As verified, in the panels (a) of Fig. 1, the attractive interspecies interaction provides complete miscibility (overlap) of the species, with maxima for the densities at the center. As shown in the panels (c), for $\delta = 1$ ($a_{12} = a_{ii}$) we have already almost complete radial phase separations of the mixture, which is further characterized in the panels (d), with $a_{12} = 200\,a_0$, where $\delta = 4/3$. These results are consistent with the ones verified in Ref. [36] for imbalanced-mass binary systems in pancake-like non-perturbed harmonic traps.

By considering linearly perturbed trap, our results for the miscibility to immiscibility transition of non-rotating ($\Omega = 0$) binary BEC are presented in Fig. 2. In the upper panels we have the surface plots with the 2D densities ($|\psi_i(x,y)|^2$) given in the $x-y$ plane, whereas in the two lower row of panels we have the corresponding density results given for $y = 0$ and $x = 0$, respectively. In all these results, we consider four values for the interspecies scattering length, such that $a_{12} = -100$ in panels (a), $a_{12} = 100$ in panels (b), $a_{12} = 150$ in panels (c), and $a_{12} = 200$ in panels (d). The linear

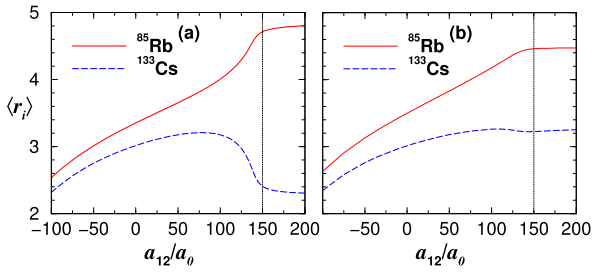

Fig. 3. The root-mean-square radii, $\langle r_i\rangle \equiv \sqrt{\langle x^2 + y^2\rangle}$ (in units of $l_\perp$), for the two components of the non-perturbed [panel (a)] and perturbed [panel (b)] harmonically trapped binary mixture, are shown as functions of a_{12} (in units of a_0), corresponding to Figs. 1 and 2 results, respectively, such that $\lambda = 10$ and $a_{ii} = 150a_0$ The vertical dotted lines (at $\delta = 1$) are close to the miscible-immiscible transition.

perturbation in the trap pushes the corresponding directly affected component along the direction of the perturbation (x-direction in our case), modifying the previous density distributions of both elements. In case of attractive interspecies interaction the effect is just in a redistribution of the overlapped mixture. However, when a_{12} is repulsive, and particularly larger than a_{11}, the perturbation affects the spatial distribution in the immiscible phase by changing the previous radial space separation to an axial one, with the two densities trapped with their maxima at distinct positions.

3.2. Space distribution, miscibility and critical rotation

In Fig. 3, by considering both unperturbed [panel (a)] and perturbed [panel (b)] harmonic traps, which have been presented in Figs. 1 and 2, we show the behavior of the dimensionless root-mean-square (rms) radii $\langle r_i\rangle \equiv \sqrt{\langle r^2\rangle_i} \equiv \sqrt{\langle x^2 + y^2\rangle_i}$ in terms of the two-body inter-species interaction a_{12}, for the two components $i = 1, 2$ of the binary mixture. Within our assumption for the intra-species a_{ii}, the corresponding δ defined by the Eq. (5) is varying from -2/3 till 4/3. As verified, the rms radius of the less-massive component (the lighter one, species 1) increases as the interspecies interaction increases, in both unperturbed and perturbed situations. On the other hand, for the unperturbed case, shown in the panel (a) of Fig. 3, the second component (the heavier one, species 2) increases as δ is increasing from negative values only till a region where $\delta \simeq 2/3$ ($a_{12} \simeq 100a_0$). For larger values of a_{12}, by entering in the more miscible region, $\langle r_2\rangle \equiv \sqrt{\langle r^2\rangle}$ starts to reduce due to the radial phase separation of the two species, which occurs as the a_{12} becomes more repulsive, saturating to some small radius at the center of the trap. By going from the unperturbed to the perturbed regime, the radial distribution is mainly modified at larger repulsive values of a_{12}, resulting in an axial spatial distribution of the two species. In this space density distribution, the confined space of component 2 turns out to be larger than before, with the panel (b) of Fig. 3 reflecting the results presented in Fig. 2.

When the system is immiscible (or less miscible), the density distribution of the mixture is no more homogeneous, with the coupled system being affected by the repulsion between the two species. Even for the unperturbed case, we observe that the peak of the density of the lighter element (^{85}Rb, $i = 1$) is deviated from the center of the trap (in case $a_{12} < 0$) to a ring surrounding the heavier element (^{133}Cs, $i = 2$), which happens when $a_{12} > a_{11}$, as observed from the panels (c) and (d) of Fig. 1. In this last situation, the component 2 becomes more strongly confined in the center of the trap due to the inter-species repulsion. In the perturbed case that we are considering, we have the density distribution affected by the trap $x-$space dislocation of the ^{85}Rb (component 1), which will also affect the ^{133}Cs (component 2) density distribution, mainly due to the inter-species interaction. So, in both the

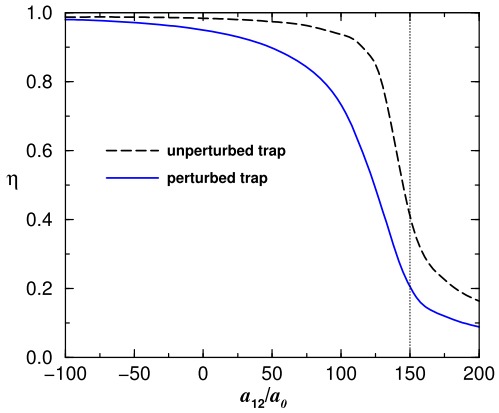

Fig. 4. Miscible-immiscible transition of non-rotating ($\Omega = 0$) binary BEC mixture in harmonic non-perturbed (dashed line) and linearly perturbed (solid line) traps, in terms of the inter-species a_{12}. The parameters are as in Figs. 1–3, with the intra-species interactions fixed to $a_{ii} = 150a_0$. The vertical dotted line at $\delta = 1$ indicates the miscible-immiscible transition for equal-mass homogeneous mixture.

cases (unperturbed and perturbed), it is relevant to verify how the density distribution is affected, by considering the miscibility of the two elements. The two-component transition from miscible to immiscible is well known as given by the condition expressed in Eq. (5)], when considering homogeneous systems [33]. However, for non-homogeneous systems it is more reliable to consider a parameter that reflects the density distribution of the species, such as the parameter η that was defined in Ref. [34]. By considering this parameter, also given by Eq. (6), a coupled system can be considered as completely miscible if $\eta = 1$ and completely immiscible if $\eta = 0$, limiting situations that can only be approached in both the cases we are considering, as verified in Fig. 4. In this figure, we show η as a function of the inter-species scattering length a_{12}, for both non-perturbed and perturbed cases. As expected, for non-perturbed harmonic trap, the transition occurs near $\delta = 1$, in agreement with Eq. (5), with the transition being softened when considering the perturbed trap. This miscibility analysis can further explain the density distributions shown in Figs. 1 and 2, in which we noticed how the miscibility is affected by the translation in the $x-$position.

The radial distributions of the condensate densities, obtained for $\Omega = 0$ and shown in the two panels of Figs. 3, are strongly affected by the miscibility of the mixture. They are relevant to estimate the critical frequency Ω_c required to generate vortices in a BEC system, as we discuss in the next. Even considering that such analysis is limited to homogeneous single component systems, in the present case of non-perturbed and perturbed coupled two-component systems it can reflect more directly the critical frequencies in regions where the coupled system is more miscible, as for attractive inter-species. From our calculations, we found appropriate to use a rotation frequency given by $\Omega = 0.7$, which is enough larger than Ω_c to help us observe vortex lattice formations in both the cases we are discussing in this work.

For the moment, let us recover from Ref. [38] the discussion related to the full-dimensional critical frequency for a single component system with mass M. By considering a BEC system in axially symmetric trap, with large number N and perpendicular Thomas-Fermi (TF) radial distribution $R_\perp$, the critical frequency was analytically derived in Ref. [39], being given by

$$\overline{\Omega}_c = \frac{5}{2}\frac{\hbar}{MR_\perp^2}\ln\left(\frac{0.671R_\perp}{\xi_0}\right), \tag{8}$$

where ξ_0 is the healing length (also called coherence length), evaluated for the density n_0 in the center of the trap. For the derivation of (8), it was assumed that the characteristic dimensions of the cloud is large compared with the coherence length at the center of the cloud, which is defined by the balance between quantum pressure and the interaction energy of the condensate [38,39], in a uniform medium. The coherence length can be expressed in terms of the scattering length a and central density n_{3D} of the gas without vortex by $\xi = 1/\sqrt{8\pi n_{3D} a}$. The expression (8) gives the *full-dimensional* critical frequencies to generate vortices in a uniform medium, expected to be valid for each single species independently, when both densities are uniformly distributed in a radial space, having the maxima at the same localization $x = y = z = 0$. When considering a coupled system, the balance between quantum pressure and the interaction energy (for each condensate) is being modified due to the miscibility of the components, such that the expression (8) is approximately valid only when the two species are miscible, not repelling each other, limited to regions where $a_{12} \lesssim a_{11}$ (in our case, more precisely, due to the mass difference, $a_{12} \leq 146.3a_0$). Within our dimensionless units, defining the perpendicular radial distribution as $\mathcal{R} \equiv (R_\perp/l_\perp)$, with the full-dimensional frequency in terms of dimensionless one being $\overline{\Omega}_c \equiv \Omega_{c,1}\omega_\perp$, from (8) we obtain

$$\Omega_{c,1} = \frac{5}{2}\frac{1}{\mathcal{R}^2}\ln\left(\frac{0.671\mathcal{R}}{\bar{\xi}_0}\right) \approx \frac{5}{2}\frac{1}{\mathcal{R}^2}\ln\left(40\,\mathcal{R}\,|\psi_{01}|\right), \tag{9}$$

where the dimensionless central healing length is $\bar{\xi}_0 \equiv \left[8\sqrt{\lambda\pi}(a_{11}/l_\perp)N_1|\psi_{01}|^2\right]^{-1/2}$, with the density of the component 1 at the origin given by $n_{0,1} = \sqrt{\lambda/\pi}|\psi_{0,1}|^2$. We are also considering our assumption for the intra-species scattering length and number of atoms, $N_1 = 10^4$, $a_{11}/l_\perp = 150/(1.89 \times 10^4)$ (such that $\xi_0/l_\perp = 0.01676/|\psi_{01}|$). Within the expectation that Eq. (9) is approximately valid for non-interacting systems, we can estimate the critical frequency and corresponding radial distribution $\mathcal{R}$, by considering in particular the point where there is no inter-species interaction, $a_{12} = 0$. In this case, the 2D central densities is found $|\psi_{0,1}|^2 = 0.019$, with the critical frequency close to 0.15, implying that $\mathcal{R} \approx 6.9$. This value for the radial distribution is about twice the value of rms radius, $\sqrt{\langle(x^2+y^2)\rangle}$, as verified by the component 1 in the panel (a) of Fig. 3.

Moreover, about the critical frequencies to generate vortices in binary coupled systems, it may be worth mentioning that further theoretical studies are demanding in order to derive an expression more general than the above (9), which can be extended to coupled systems and reflect the computed results displayed in Fig. 5. For such, one can rely on some previous analytical studies (done for single components), in which the hydrodynamic equations have been applied under the TF approximation, as in Refs. [38,39], by considering the two regimes, with miscible [15] and immiscible [33] phases for the coupled mixture.

In order to calculate the threshold rotation, we should emphasize that it will be helpful the random phase in the initial wave function. Without random phase, a single vortex continues to exist for $\Omega < \Omega_c$. At the critical rotation frequency (Ω_c) a single vortex enters into the condensate. When the rotation frequency is significantly higher than Ω_c, then more vortices will enter into the condensate. The Ω_c required to create the single vortex in rotating condensates depends on the interaction strength (that determines the radius) and the trap geometry (pancake or cigar). One needs larger Ω_c for more attractive interaction, which shrinks the condensate radius. In contrast, the repulsive interaction expands the radius, resulting in smaller Ω_c. Our main results on the critical frequencies are summarized in the Fig. 5, for both unperturbed [panel (a)] and perturbed [panel (b)] cases. By looking the results for the unperturbed case, given in the panel (a), we notice that

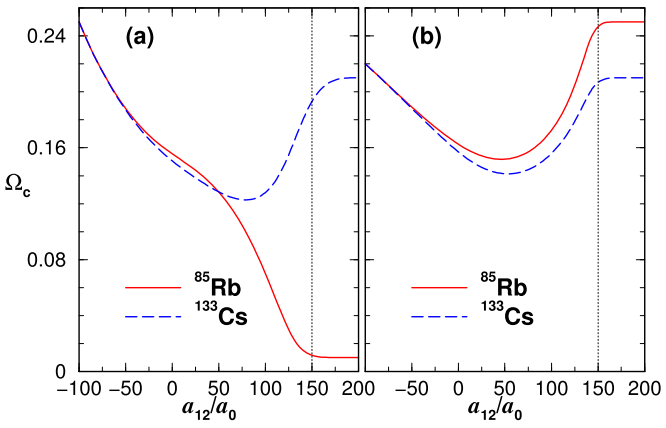

Fig. 5. In this figure, the lines (solid-red for ^{85}Rb, dashed-blue for ^{133}Cs) are representing the minimum critical frequency Ω_c (as functions of the inter-species a_{12}), in order to generate vortices, which can exist only above the corresponding curves ($\Omega \geq \Omega_c$). The non-perturbed and perturbed coupled systems are, respectively, in the left and right panels. The vertical dotted lines (both panels) are close to the miscibility transition for homogeneous systems. These results can be qualitatively compared with the ones respectively shown in Fig. 3 for the radii. In all the cases, $a_{ii} = 150a_0$, with Ω given in units of $\omega_\perp$.

Ω_c of both the first and second component are about the same until $a_{12} \geq 60a_0$, when start deviating from each other. By increasing the inter-species interaction a_{12}, the critical frequency of the first component Ω_{c_1} diminishes due to its radial expansion, which makes more favorable to generate vortices with smaller rotation frequency, saturating at $a_{12} \approx 150a_0$ ($\delta = 1$). This result can be directly associated with the corresponding radial distribution shown in Fig. 3, in which we do not find big difference in the radius for a_{12} between $150a_0$ and $200a_0$. In contrast, Ω_{c_2} starts to increase from $a_{12} \geq 100a_0$, reflecting the respective reduction in the radial distribution of the component 2.

Next, we consider the Ω_c for the case of binary mixtures, when the trap of component 1 is linearly shifted in the $x-$direction. In this case, the critical frequencies of both components are about the same as the ones obtained when in the presence of attractive inter-species interaction. The repulsive inter-species interaction provides axial phase separation, introducing some small difference between Ω_{c_1} and Ω_{c_2} of the mixture. In this case, from the radial distribution of both systems, shown in Fig. 3, with $\sqrt{\langle r_1^2 \rangle} > \sqrt{\langle r_2^2 \rangle}$, one should expect $\Omega_{c_1} < \Omega_{c_2}$. However, we are observing that $\Omega_{c_1} > \Omega_{c_2}$, which can be explained by the fact that the first component density have its maximum distribution located a bit far from the center of the trap, as verified from panels (d) of Fig. 2, due to the immiscibility of the mixture.

In order to verify how the vortices are being generated when we are close to the critical limit of rotation, we present some results in Fig. 6, by considering, respectively, both the unperturbed and perturbed trap cases. For these sample results, the densities for the species $i = 1, 2$ are represented in the upper part of the figure by two sets with four panels [(a_i) and (b_i)], in which the left set is for the unperturbed case, with the right set referring to the perturbed case. Correspondingly, we have the respective phases shown in two sets with four panels [(c_i) and (d_i)] in the lower part of the figure. For the non-perturbed case, shown in the left sets of Fig. 6 (densities and phases), we are considering the non-interacting case $a_{12} = 0$ in the panels (a_i) and (c_i), with rotation frequency $\Omega = 0.17$; whereas in the panels (b_i) and (d_i) we have $a_{12} = 150a_0$ ($\delta = 1$) with $\Omega = 0.22$. In particular, for the case with $\delta = 1$, in which from Fig. 5 we have $\Omega_c \sim 0.01$, one can verify the occurrence of vortices in the low-density region of component 1 [panel (b_1)] from the corresponding phase diagram, given in the panel (d_1). Analogously, for the perturbed case

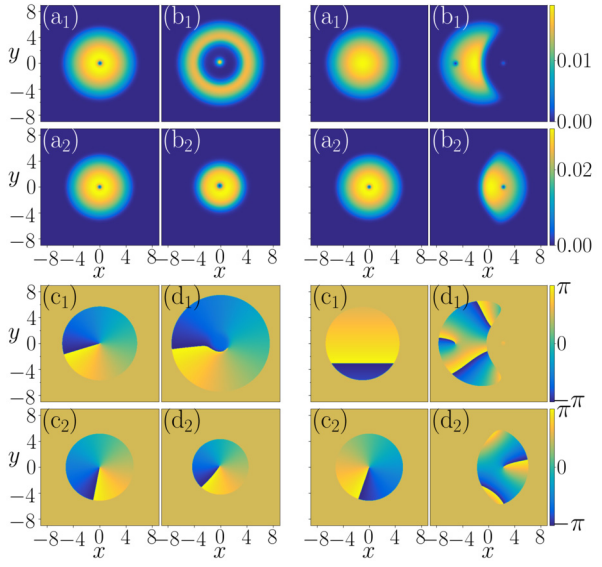

Fig. 6. Sample results of 2D densities $|\psi_{i=1,2}(x, y)|^2$ (units $l_\perp^{-2}$) in the (x, y) plane (space unit $l_\perp$) for the coupled non-perturbed (left upper set of panels) and linear perturbed (right upper set of panels) systems. Correspondingly, the phase diagrams are shown in the next two lower rows of panels (c_i) and (d_i). In the non-perturbed cases (left set), the panels (a_i) and (c_i) are for $a_{12} = 0$ ($\delta = 0$) with $\Omega = 0.17$, with panels (b_i) and (d_i) for $a_{12} = 150a_0$ ($\delta = 1$) with $\Omega = 0.22$. In the perturbed case (right set), the panels (a_i) and (c_i) are for $a_{12} = 0$ ($\delta = 0$) with $\Omega = 0.16$, with panels (b_i) and (d_i) for $a_{12} = 150a_0$ ($\delta = 1$) with $\Omega = 0.25$. In all the cases, $a_{ii} = 150a_0$, with trap aspect ratio $\lambda = 10$.

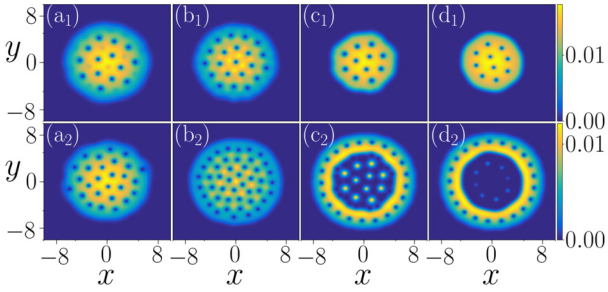

Fig. 7. Vortex-lattice structures in the 2D coupled densities, $|\psi_i(x, y)|^2$ (units $l_\perp^{-2}$), for the binary mixture ^{85}Rb$-^{133}$Cs, using pancake-like harmonic trap with aspect ratio $\lambda = 10$ and rotation frequency $\Omega = 0.7\omega_\perp$, in the (x, y) plane (space unit $l_\perp$). With $a_{ii} = 150a_0$, the a_{12} goes from attractive $a_{12} = -50a_0$ [panels (a_i)], providing complete overlap of the densities; to three repulsive cases, with $a_{12} = 50a_0$ [panels (b_i)], $150a_0$ [panels (c_i)] and $200a_0$ [panels (d_i)], in which (c_i) and (d_i) are in almost complete immiscible radial separation, with the lighter element occupying the center of the trap.

shown in the right sets of Fig. 6 (densities and phases), we have $a_{12} = 0$ with $\Omega = 0.16$ in the panels (a_i) and (c_i); with the repulsive case, $a_{12} = 150a_0$ ($\delta = 1$), with $\Omega = 0.25$, being shown in the panels (a_i) and (c_i). As shown in both the cases represented in the Fig. 6, with $a_{12} = 150a_0$, we have already entered in the immiscible regime of the mixtures. Radial separation of the mixture is verified in case we have non-perturbed trap system, with the lighter element (^{85}Rb) surrounding the heavier element (^{133}Cs), which is in the center. These results follow in correspondence with the ones verified in Figs. 1 and 3(a), when $\Omega = 0$, for the relative position of the element densities in the trap.

Next, we consider a larger and fixed rotation, given by $\Omega = 0.7$, which has shown to be enough to create some lattice patterns of vortices in both components of the mixture. These results are shown in Fig. 7, for the unperturbed case; and in Fig. 8 for the perturbed case. In both the cases, we assume four values for the two-body interaction, going from the attractive cases, $a_{12} = -50a_0$

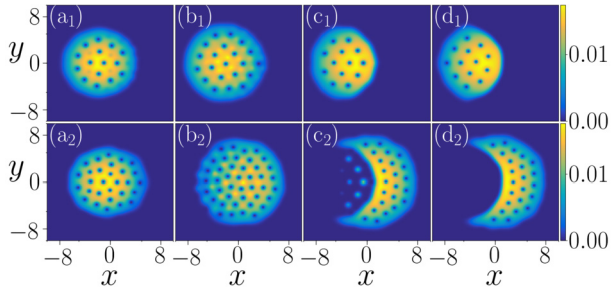

Fig. 8. This figure shows the vortex-lattice structures corresponding to the results shown in Fig. 7, when the harmonic trap of component 1 is perturbed in the $x-$direction ($\nu_1 = 1, \nu_2 = 0$). Except for the perturbation, the other parameters are as in Fig. 7, with $\Omega = 0.7\omega_\perp$, $\lambda = 10$, and with $a_{12} = -50\,a_0$ [panels (a_i)], $a_{12} = 50\,a_0$ [panels (b_i)], $150\,a_0$ [panels (c_i)] and $200\,a_0$ [panels (d_i)]. The almost complete immiscible condition (c_i) and (d_i) are providing space separation with both species having their maxima side-by-side in the $x-$direction.

($\delta = -1/3$), to three repulsive ones, with $a_{12} = 50a_0$ ($\delta = 1/3$), $a_{12} = 150a_0$ ($\delta = 1$), and $a_{12} = 200a_0$ ($\delta = 4/3$). As been clearly verified in both figures, the cases with $\delta \geq 1$ shown in the panels (c_i) and (d_i) correspond to the immiscible cases. Here, even for the unperturbed case, we can already observe a striking result due to the mass-imbalance sensibility of the mixture which is emerging as the rotation frequency is increased. As observed from Fig. 1, where we have $\Omega = 0$ and from upper set of Fig. 6 where the rotation is quite small, in particular for the case with $\delta \geq 1$, we have radial space separation, the coupled element interchange their spatial separated positions for higher frequencies, such that with $\Omega = 0.7$ we can already verify the lighter element occupying the center of the trap, with the heavier element surrounding the first (in opposite locations, as compared with the case of low or zero rotation frequency). Due to the immiscibility and confinement to a smaller radius, the number of vortices of the component 1, which is in the center, becomes smaller than the number of vortices appearing in the component 2.

For the perturbed case, shown in Fig. 8, the $x-$dislocation of the component 1 density affects the radial-shaped structure separation of the mixture, such that the coupled system turns out to display an axial phase-space separation with the species 1 shifted from the center. Due to the fact that component 1 is located in a smaller radius, this translation in the $x-$position will also affect the component 2, which was surrounding the first before the perturbation, as verified in particular for the immiscible regime shown by the panels (c_i) and (d_i). In conclusion, the Figs. 7 and 8 are presenting our main results concerning the mass-imbalance sensibility of the mixture when considering the relative space separation of the two components, particularly for repulsive inter-species interaction larger than the intra-species ones. These results provide further support to the conclusions obtained in Ref. [20] about the relevance of the mass difference in a binary rotating mixture.

4. Summary and discussion

We have studied the ^{85}Rb-^{133}Cs binary BEC mixture in rotating non-perturbed and perturbed harmonic traps. First, we examine the equilibrium non-rotating ground states by changing the inter-species contact interaction strength. Due to the mass-imbalance of the mixture, we observe a radial phase separation between the two confined species when the inter-species interaction a_{12} is repulsive and larger than the corresponding intra-species $a_{11} = a_{22}$, with both species confined in unperturbed harmonic traps. The mean-square radii of the binary BEC mixtures are obtained by verifying that $\langle r_1^2 \rangle$ of the first component (the lighter one) increases as a_{12} becomes more repulsive, with $\langle r_2^2 \rangle$ (of the heavier element) reverting its increasing behavior as a_{12} approaches the value of a_{ii}, in agreement with the mass-dependent condition (5) for the miscible-immiscible transition of homogeneous mixtures. This behavior occurs due to the strong inter-species repulsion. Next, to study the rotational properties of the ^{85}Rb-^{133}Cs BEC mixture, we introduce a non-zero angular momentum rotation frequency Ω (in units of the transversal trap frequency $\omega_{1,\perp}$), estimating the corresponding critical values Ω_{c_i} to observe a single vortex in the binary mixture. In agreement with the radial distributions given by the rms radii, the Ω_{c_1} continuously decreases as a_{12} becomes more repulsive, till reaching a minimum frequency value for $a_{12} > a_{ii}$. However, in the case of the heavier species, as a_{12} increases, the initial decreasing behavior of Ω_{c_2} reaches a minimum in correspondence with the radial behavior. After that, Ω_{c_2} starts increasing till a saturating limit for $a_{12} > a_{ii}$. This tendency that occurs for the non-perturbed coupled system is consistent with the immiscibility of the coupled mixture, such that the two species start to repel each other strongly for $\delta > 1$. Without a perturbation in the trap, the distribution of the two densities becomes radially separated in the immiscible regime, with the heavier element located in the inner part, such that a larger value of Ω is needed to start vortex generation. A linear perturbation applied to the element 1 will affect this radial distribution, which happens in the immiscible regime, having both element distributions with their maxima at separate positions, implying in having their density with similar side-by-side distributions. So, in both the cases, Ω_{c_i} decreases in the miscible region as a_{12} increases, till some independent minima which occur when the system starts becoming immiscible, saturating at some value $a_{12} > a_{ii}$.

When the coupled system is confined by unperturbed harmonic traps, in this immiscible regime we have the less massive species surrounding the more massive one, for the non-rotating case $\Omega = 0$ or when the rotation is not large enough. As we increase the frequency of the rotation, a transition occurs resulting in an interchange on the radial space distribution of the mixture. As shown, in the immiscible regime, for $\Omega = 0.7$ one can already verify that the peak of the density of the more massive element is no more in the center, but outside the center of the trap, in a ring surrounding the lighter one, which has moved to the center. The less massive element, in this case, becomes confined in the inner center region, under the pressure of the more massive element. This is a relevant "centrifugal effect" that, in some way, could be expected, as been relevant in order to calibrate experimental realizations with rotating mass-imbalanced BEC mixtures, such as ^{85}Rb-^{133}Cs. The effect can be further explored for different mass-imbalanced systems, by considering the corresponding frequencies for the transitions.

By studying the effect of linear perturbation (along the $x-$direction) in the trap of one of the mass-imbalanced components (which we choose the lighter one of the ^{85}Rb-^{133}Cs mixture), we are providing some more elements for a possible simple experimental realization in cold-atom laboratories, with rotating mass-imbalanced binary non-dipolar systems. The presence of linear perturbation in the trap pushes the first component along that direction, altering the density distribution and the corresponding associated vortices in the rotating regime. In the attractive case and in the miscible regime ($a_{12} < a_{ii}$), we just observe some expected changes in the vortex patterns, already explored in several other works. However, it is in the more repulsive case (immiscible regime) that we have verified the more significant changes, with the previous radial space separation being changed to a side-by-side phase separation between the elements of the mixture. Within such side-by-side spatial separation in the immiscible regime ($\delta > 1$), both densities have their trapped regions basically governed by their mass differences. For both elements, the vortex-pattern structures are distributed within the corresponding available spatial regions.

Declaration of competing interest

We wish to confirm that there are no known conflicts of interest associated with this publication and there has been no significant financial support for this work that could have influenced its outcome.

Acknowledgements

The authors acknowledge partial support received from Conselho Nacional de Desenvolvimento Científico e Tecnológico (CNPq) [Procs. 304469/2019-0 (LT), 153522/2018-6 (RKK) and 306920/2018-2 (AG)], Fundação de Amparo à Pesquisa do Estado de São Paulo (FAPESP) [Contracts 2016/14120-6 (LT), 2016/17612-7 (AG)]. RKK also acknowledge support from Marsden Fund (Contract UOO1726).

References

[1] C.J. Myatt, E.A. Burt, R.W. Ghrist, E.A. Cornell, C.E. Wieman, Phys. Rev. Lett. 78 (1997) 586.
[2] M.R. Matthews, B.P. Anderson, P.C. Haljan, D.S. Hall, C.E. Wieman, E.A. Cornell, Phys. Rev. Lett. 83 (1999) 2498.
[3] S.B. Papp, J.M. Pino, C.E. Wieman, Phys. Rev. Lett. 101 (2008) 040402.
[4] S. Sugawa, R. Yamazaki, S. Taie, Y. Takahashi, Phys. Rev. A 84 (2011) 011610.
[5] G. Modugno, M. Modugno, F. Riboli, G. Roati, M. Inguscio, Phys. Rev. Lett. 89 (2002) 190404.
[6] G. Thalhammer, G. Barontini, L. De Sarlo, J. Catani, F. Minardi, M. Inguscio, Phys. Rev. Lett. 100 (2008) 210402.
[7] M. Brtka, A. Gammal, B.A. Malomed, Phys. Rev. A 82 (2010) 053610.
[8] D.J. McCarron, H.W. Cho, D.L. Jenkin, M.P. Köppinger, S.L. Cornish, Phys. Rev. A 84 (2011) 011603(R).
[9] A.D. Lercher, T. Takekoshi, M. Debatin, B. Schuster, R. Rameshan, F. Ferlaino, R. Grimm, H.-C. Nägerl, Eur. Phys. J. D 65 (2011) 3.
[10] B. Pasquiou, A. Bayerle, S.M. Tzanova, S. Stellmer, J. Szczepkowski, M. Parigger, R. Grimm, F. Schreck, Phys. Rev. A 88 (2013) 023601.
[11] L. Wacker, N.B. Jørgensen, D. Birkmose, R. Horchani, W. Ertmer, C. Klempt, N. Winter, J. Sherson, J.J. Arlt, Phys. Rev. A 92 (2015) 053602.
[12] C.-F. Liu, H. Fan, S.-C. Gou, W.-M. Liu, Sci. Rep. 4 (2015) 4224.
[13] K.L. Lee, N.B. Jørgensen, I.-K. Liu, L. Wacker, J.J. Arlt, N.P. Proukakis, Phys. Rev. A 94 (2016) 013602.
[14] A. Trautmann, P. Ilzhöfer, G. Durastante, C. Politi, M. Sohmen, M.J. Mark, F. Ferlaino, Phys. Rev. Lett. 121 (2018) 213601.
[15] J. Polo, W. Ahufinger, P. Mason, S. Sridhar, T.P. Billam, S.A. Gardiner, Phys. Rev. A 91 (2015) 053626.
[16] P. Kuopanportti, Y.M. Liu, Y.Z. He, C.G. Bao, J. Phys. B, At. Mol. Opt. Phys. 52 (2019) 015001.
[17] A.E. Leanhardt, Y. Shin, D. Kielpinski, D.E. Pritchard, W. Ketterle, Phys. Rev. Lett. 90 (2003) 140403.
[18] A.M. Martin, N.G. Marchant, D.H.J. O'Dell, N.G. Parker, J. Phys. Condens. Matter 29 (2017) 103004.
[19] S.B. Prasad, T. Bland, B.C. Mulkerin, N.G. Parker, A.M. Martin, Phys. Rev. Lett. 100 (2019) 023625.
[20] R.K. Kumar, L. Tomio, A. Gammal, Phys. Rev. A 99 (2019) 043606.
[21] A.L. Fetter, Rev. Mod. Phys. 81 (2009) 647.
[22] E.J. Mueller, T.L. Ho, Phys. Rev. Lett. 88 (2002) 180403.
[23] K. Kasamatsu, M. Tsubota, M. Ueda, Phys. Rev. Lett. 91 (2003) 150406.
[24] K. Kasamatsu, M. Tsubota, Phys. Rev. A 79 (2009) 023606.
[25] P. Mason, A. Aftalion, Phys. Rev. A 84 (2011) 033611.
[26] R.K. Kumar, L. Tomio, B.A. Malomed, A. Gammal, Phys. Rev. A 96 (2017) 063624.
[27] Z. Chen, Y. Li, N.P. Proukakis, B.A. Malomed, New J. Phys. 21 (2019) 073058.
[28] A. Richaud, V. Penna, R. Mayol, M. Guilleumas, Phys. Rev. A 101 (2020) 013630.
[29] K. Mukherjee, S.I. Mistakidis, P.G. Kevrekidis, P. Schmelcher, J. Phys. B, At. Mol. Opt. Phys. 53 (2020) 055302.
[30] R.W. Pattinson, T.P. Billam, S.A. Gardiner, D.J. McCarron, H.W. Cho, S.L. Cornish, N.G. Parker, N.P. Proukakis, Phys. Rev. A 87 (2013) 013625.
[31] T. Weber, J. Herbig, M. Mark, H.-C. Nägerl, R. Grimm, Science 299 (2003) 232.
[32] S.K. Adhikari, Commun. Nonlinear Sci. Numer. Simul. 71 (2019) 212.
[33] P. Ao, S.T. Chui, Phys. Rev. A 58 (1998) 4836.
[34] R.K. Kumar, P. Muruganandam, L. Tomio, A. Gammal, J. Phys. Commun. 1 (2017) 035012.
[35] L. Wen, W.M. Liu, Y. Cai, J.M. Zhang, J. Hu, Phys. Rev. A 85 (2012) 043602.
[36] S. Bandyopadhyay, A. Roy, D. Angom, Phys. Rev. A 96 (2017) 043603.
[37] R. Kishor Kumar, V. Lončar, P. Muruganandam, S.K. Adhikari, A. Balaž, Comput. Phys. Commun. 240 (2019) 74.
[38] F. Dalfovo, S. Giorgini, L.P. Pitaevski, S. Stringari, Rev. Mod. Phys. 71 (1999) 463.
[39] E. Lundh, C.J. Pethick, H. Smith, Phys. Rev. A 55 (1997) 2126.